Flow behavior of cohesive and frictional fine powders

S. Luding
Particle Technology, DelftChemTech, TU Delft, Julianalaan 136, 2628 BL Delft, Netherlands

Rostyslav Tykhoniuk, Jürgen Tomas
Mechanische Verfahrenstechnik, Otto-von-Guericke-Universität Magdeburg, Postfach 4120, 39016 Magdeburg, Germany

Lars Heim, Michael Kappl, Hans-Jürgen Butt
Max-Planck-Institut für Polymerforschung, Ackermannweg 10, 55128 Mainz, Germany

ABSTRACT: Continuum mechanical models and appropriate measuring methods are applied to describe the flow behaviour of cohesive powders and, for example, for practical design of process apparatus as silos. Studies of the particle mechanics can provide a better physical "microscopic" understanding of the essential constitutive functions of a powder "continuum". With the discrete element method (DEM), a tool is available that allows to consider the details of the contact and adhesion forces for each particle contact. Based on both experimental and empirical observations, a general law is introduced, involving an irreversible (plastic), contact flattening (that leads to an increase of adhesion force for increasing flattening). The DEM results show an elastic regime, yielding and steady-state flow of a two-dimensional model powder

1 INTRODUCTION

Given the particle geometry and their interaction forces, the flow behavior of powders under large deformations can be studied, using the discrete element method (DEM), a convenient tool to gain insight into the evolution of, e.g., shear bands. Powders are typically inhomogeneous, disordered, and anisotropic on a "microscopic" scale [1-3], where the typical microscopic size is the particle size. Irregular random arrays respond to deformations via inhomogeneous and anisotropic rearrangements and stress-response. An initially isotropic contact network becomes anisotropic before the structure of the network reaches its limit of stability, i.e., the yield stress. Before the peak, one has softening, and beyond weakening is obtained [2-5], which is typical for over-consolidated powders. Our work complements recent studies on shear band formation in frictional-cohesive granular media [4-8], for micro- and macro-modeling [9,10], and in various systems [11-14] for different materials.

Here, only spherical particles are used, as opposed to non-spherical objects like polygons [10], where roughness can also be mimicked by additional torques [15]. The recently developed micro-macro transition procedures [6-13] aim at a better understand of the macroscopic powder flow behavior on microscopic foundations. Besides the experimental verification of the simulation results [14], the formulation of constitutive relations in the framework of continuum theory is the great challenge. One promising material model, especially for sand is the hypoplastic theory [16-20], for which the material parameters can be determined experimentally, or from DEM simulations, as shown in this study for some cases.

2 MODEL

2.1 *DEM and the contact laws*

The elementary units of granular materials, the "mesoscopic" particles, locally – at the contact point – deform under stress. The realistic modeling of the deformations inside is too much effort, so that we relate the interaction force only to the overlap δ of two particles, see Fig. 1. As a further simplification, these two particles interact only if they are in contact (short range forces), and the force between them is decomposed into a normal and a tangential part.

Figure 1: Two particle contact with overlap δ.

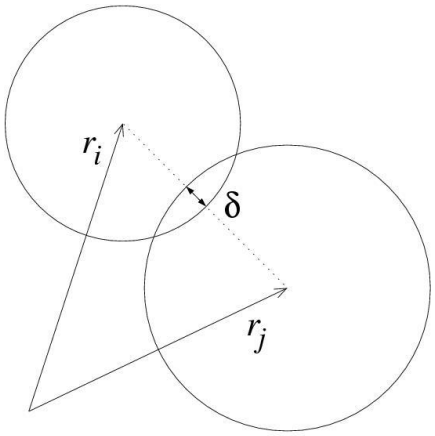

The *normal force* is, in the simplest case, a linear spring that takes care of repulsion, and a linear dashpot that accounts for dissipation during contact. Here, we propose a new model that takes into account plastic contact deformation and cohesion (attractive forces). The force displacement scheme is shown in Figure 2.

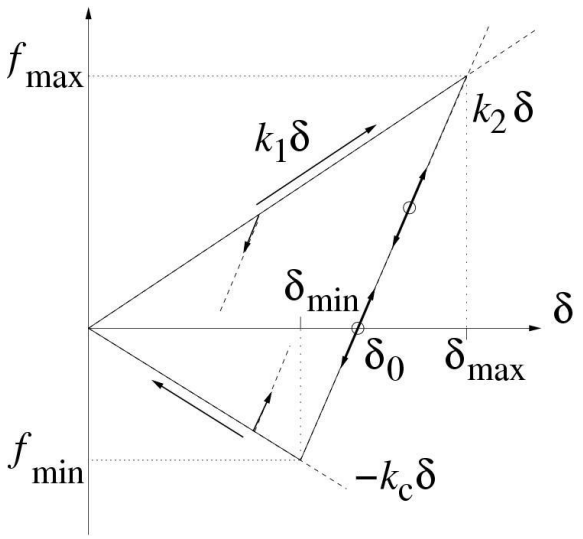

Figure 2: Force displacement law for the DEM simulations.

For initial loading of the contact, the force increases linearly with stiffness k_1, which takes care of perfect-plastic repulsion [8,9,12]. In addition, a linear dashpot accounts for dissipation during contact. Elasticity at the contact level is added by a spring, with a larger stiffness, k_2, for un- and re-loading, so that the stiffness increases due to the irreversible, plastic contact deformation. Cohesion (or an attractive adhesion force) between the contacts comes into the model by a "cohesive stiffness" k_c, which allows for attractive forces (here negative) up to a minimal (maximal attractive) force f_{min}. Cast into an equation, the normal force on particle i is:

$$\vec{f}_0^{\,n} = -\gamma_n \vec{v}_n + \hat{n}\begin{cases} k_1\delta & \text{for 1}^{\text{st}}\text{ loading} \\ k_2(\delta-\delta_0) & \text{for un-/re-loading} \\ -k_c\delta & \text{for un-loading} \end{cases}$$

with the normal direction unit vector $\hat{n}$ pointing from the center of particle j to particle i, the normal relative velocity $\vec{v}_n$ (as defined below) and the viscous dissipation parameter γ_n.

The *tangential force* involves dissipation due to Coulomb friction, but also some tangential elasticity that allows for stick-slip behavior on the contact level [4,9,10,13,14]. The implementation used here is slightly different from those presented in the literature, in so far that an implementation in two and three dimensions is equally simple and also static and dynamic friction can be used with different values for the respective coefficients.

In the static case, the tangential force is coupled to the normal force via Coulombs law, i.e. $f^t \le \mu_s f^n$, where for the limit sliding case one has the dynamic friction with $f^t = \mu_d f^n$.

The dynamic and the static friction coefficients follow, in general, the relation $\mu_d \le \mu_s$. However, for the following simulations, we will apply $\mu = \mu_d = \mu_s$. The static case requires an elastic spring in order to allow for a restoring force, i.e. a non-zero remaining tangential force in static equilibrium due to activated Coulomb friction.

If a contact exists with non-zero normal force, the tangential force is active too, and we project the tangential spring into the actual tangential plane. This is necessary, since the frame of reference of the contact may have slightly rotated since the last time-step. $\vec{\xi} = \vec{\xi}' - \hat{n}(\hat{n}\cdot\vec{\xi}')$, where $\vec{\xi}'$ is the old spring from the last iteration, and $\hat{n}$ is the normal unit vector. This action is relevant only for an already existing spring; if the spring is new, the tangential spring-length is zero, but its change is well defined anyway. The tangential velocity is $\vec{v}_t = \vec{v}_{ij} - \hat{n}(\hat{n}\cdot\vec{v}_{ij})$, with the total relative velocity of the contact surfaces of the two particles i and j:

$$\vec{v}_{ij} = \vec{v}_i - \vec{v}_j + a_i\hat{n}\times\vec{\omega}_i + a_j\hat{n}\times\vec{\omega}_j \,. \qquad (1)$$

Next, we calculate the tangential test-force as the sum of the tangential spring and a tangential viscous force (in analogy to the normal viscous force)

$$\vec{f}_0^{\,t} = -k_t\vec{\xi} - \gamma_t\vec{v}_t \,, \qquad (2)$$

with the tangential spring stiffness k_t and a tangential dissipation parameter γ_t. As long as $\left|\vec{f}_0^{\,t}\right| \le f_C^s$, with $f_C^s = \mu_s f^n$, one has static friction and, on the other hand, if $\left|\vec{f}_0^{\,t}\right| > f_C^s$, sliding, dynamic friction is active, with $f_C^d = \mu_d f^n$. As soon as $\left|\vec{f}_0^{\,t}\right| \le f_C^s$ is reached again, static friction is activated.

In the former, *static case*, the tangential spring is incremented $\vec{\xi}' = \vec{\xi} + \vec{v}_t\Delta t_{MD}$, with the time step Δt_{MD} of the DEM simulation. The new value of $\vec{\xi}'$ is to be used in the next iteration and the tangential force as defined above is used.

In the latter, *sliding case*, the tangential spring is adjusted to a length, which is consistent with Coulombs condition

$$\vec{\xi}' = -(1/k_t)\left(f_C^d\,\hat{t} + \gamma_t\vec{v}_t\right), \qquad (3)$$

with the tangential unit vector, $\hat{t} = \vec{f}_0^{\,t}\Big/\left|\vec{f}_0^{\,t}\right|$, defined by the direction of the tangential test force above, and thus the magnitude of the Coulomb force is used. Inserting the new spring length into the test force definition leads to $f_0^t = \left|-k_t\vec{\xi}' - \gamma_t\vec{v}_t\right| \approx f_C^d$

Note that $\vec{f}_0^{\,t}$ and $\vec{v}_t$ are not necessarily parallel in three dimensions. However, the mapping works always, rotating the new spring such that the direction of the frictional force is unchanged and, at the same time, limiting the spring in length according to Coulombs law.

In short notation the tangential force on particle i reads $\vec{f}^t = \min\left(f_C, \left\|\vec{f}_0^t\right\|\right)\hat{t}$, where $f_C = f_C^d$ for sliding and $f_C = f_C^s$ for sticking contacts, as defined above.

Note that the tangential force described above is identical to the classical Cundall-Strack spring only in the limits $\mu = \mu_d = \mu_s$ and $\gamma_t = 0$. The sequence of computations and the definitions and mappings into the tangential direction, however, is new to our knowledge in so far that it can be easily generalized to three dimensions.

If all forces acting on a selected spherical particle (either from other particles, from boundaries or from external forces) are known, the problem is reduced to the integration of Newton's equations of motion for the translational and rotational degrees of freedom:

$$m_i \frac{\mathrm{d}^2}{\mathrm{d}t^2}\vec{r}_i = \vec{f}_i + m_i\vec{g} \quad \text{and} \quad I_i \frac{\mathrm{d}}{\mathrm{d}t}\vec{\omega}_i = \vec{t}_i \qquad (4)$$

with the gravitational acceleration $\vec{g}$, mass m_i of the particle, its position $\vec{r}_i$, the total force $\vec{f}_i = \sum_c \vec{f}_i^c$, acting on it due to contacts with other particles or with the walls, its moment of inertia I_i, its angular velocity $\vec{\omega}_i$, and the total torque $\vec{t}_i = \sum_c \vec{l}_i^c \times \vec{f}_i^c$, with the center-contact "branch" vector $\vec{l}_i^c$.

2.2 Model System

The simulations with the discrete element model [4-10] use a two-dimensional bi-axial box, see Fig. 3, where the left and bottom walls are fixed. Stress- or strain-controlled deformation is applied to the side- and top-walls, respectively. In a typical simulation, the top wall is slowly shifted downwards, while the right wall moves, controlled by a constant stress p_x, responding on the forces exerted on it by the material in the box. The motion of the top-wall follows a cosine function, in order to allow for a smooth start-up and finish of the motion so that shocks and inertia effects are reduced, however, the shape of the function is arbitrary as long as it is smooth.

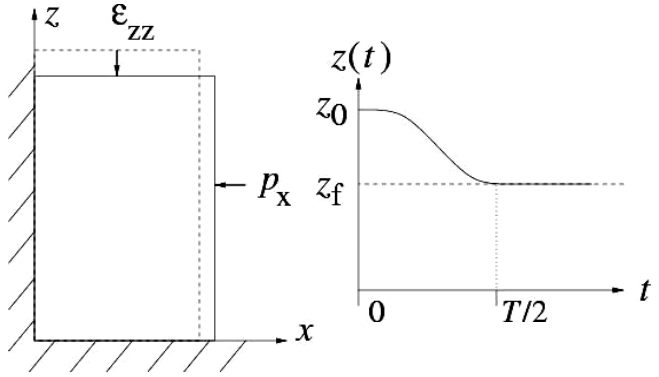

Figure 3: (Left) Schematic drawing of the model system. (Right) Position of the top-wall as function of time for the strain-controlled situation.

2.3 Initial conditions

Initially, the particles are randomly distributed in a huge box, with rather low overall density. Then the box is compressed by defining an external pressure p, in order to achieve an isotropic initial condition with kinetic energy much smaller than the potential energy stored in the contacts. Starting from this relaxed, isotropic configuration, the strain ε_{zz} is applied to the top wall and the response of the system is examined.

3 RESULTS

The system examined in the following contains N=1950 particles with radii randomly drawn from a homogeneous distribution with minimum 0.5 mm and maximum 1.5 mm. The friction coefficient used in the two-dimensional simulations is μ=0.5. The total mass of the particles in the system is about 0.02 kg. If not explicitly mentioned, the material stiffness parameters are k_2=10^5 N/m, k_1/k_2=1/2, and the contact-viscosity is 0.1 kg/s. The eigen-frequency of the particle contact is hence typically 10^{-5} s so that an integration time-step of 2.10^{-7} s is used, in order to allow for a "safe" integration [1,12].

3.1 Bi-axial test with varying cohesion

In Fig. 4 (top), the volume change of a typical simulation with cohesion, but without friction, μ=0, shows first compression, then dilatancy. The stronger the cohesion, the more the material can be compressed, while the dilatancy is almost un-affected by cohesion. At the same time, the stress response (the index zz denotes the vertical stress) becomes more and more anisotropic, i.e., the vertical stress increases until it reaches a maximum, while the horizontal stress remains constant. After the peak, softening behavior and large fluctuations are evidenced. The peak stress value increases with the microscopic cohesion or adhesion force f_{min}.

From the macroscopic point of view, the flow behavior of the system can be examined by plotting Mohr-circles for different confining pressures (left-most point on the circle) and for the maximum stress (right-most point), see Fig. 5. The tangent to these circles can be seen as the flow function for the peak stress, which corresponds to a yield locus of an over-consolidated packing. It is linear for the examined parameters with a slope slightly larger than expected from the microscopic friction at the contacts alone. If no microscopic friction is active, a friction angle of about 13° is obtained (0° expected).

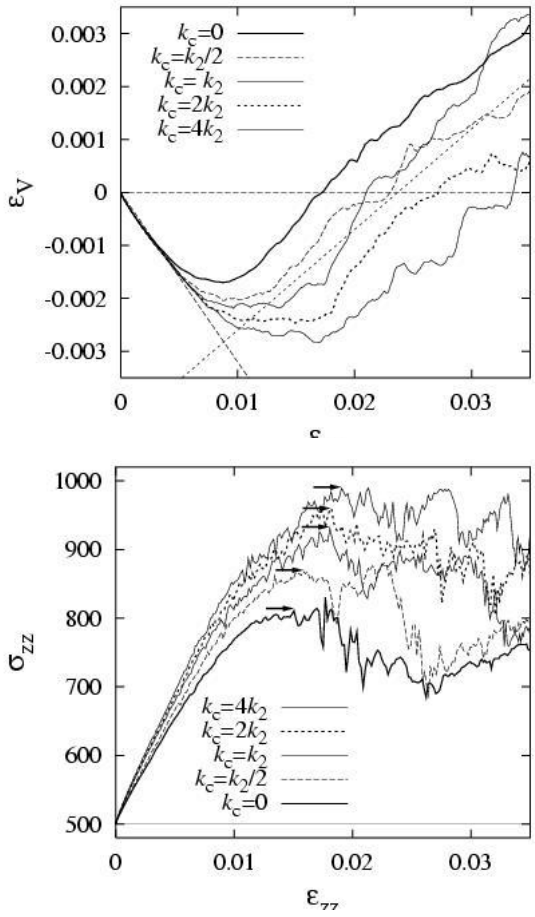

Figure 4: Volumetric strain (top) and stresses (bottom) for a bi-axial box simulation with side pressure p=500.

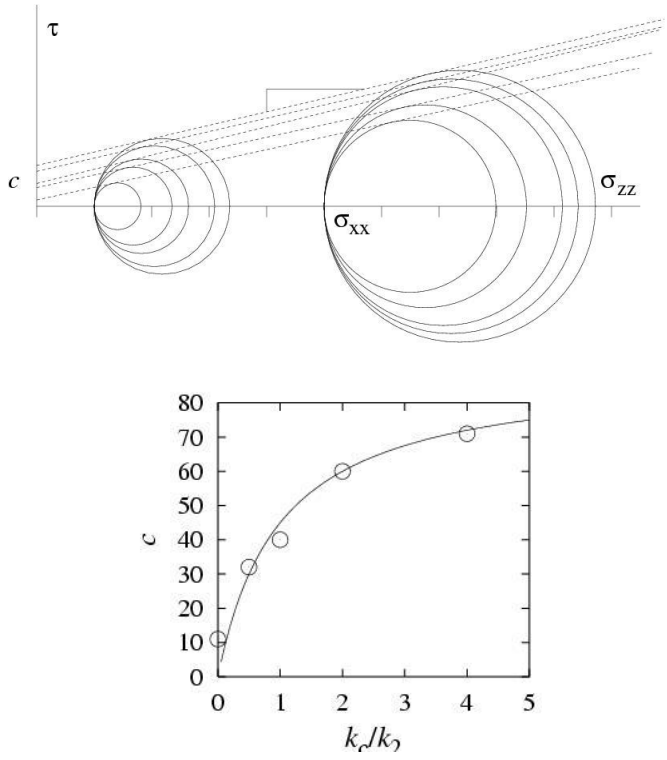

Figure 5: (top) Mohr circle representation of the flow function at maximum stress for cohesion and no friction (bottom). Macroscopic cohesion as function of the microscopic cohesive strength. The points are taken from the flow functions, the line corresponds to the analytical expression for the maximal attractive force as function of k_c/k_2.

3.2 Bi-axial test with varying pressure

In Fig. 6 (top), the volume change of a typical simulation shows first compression, then dilatancy, and eventually a very weak change at very large deformations, up to 20 per-cent. At the same time, the stress response, in Fig. 6 (bottom) (where the indices xx and zz denote horizontal and vertical stresses, respectively), shows elastic, softening, and critical state flow behavior.

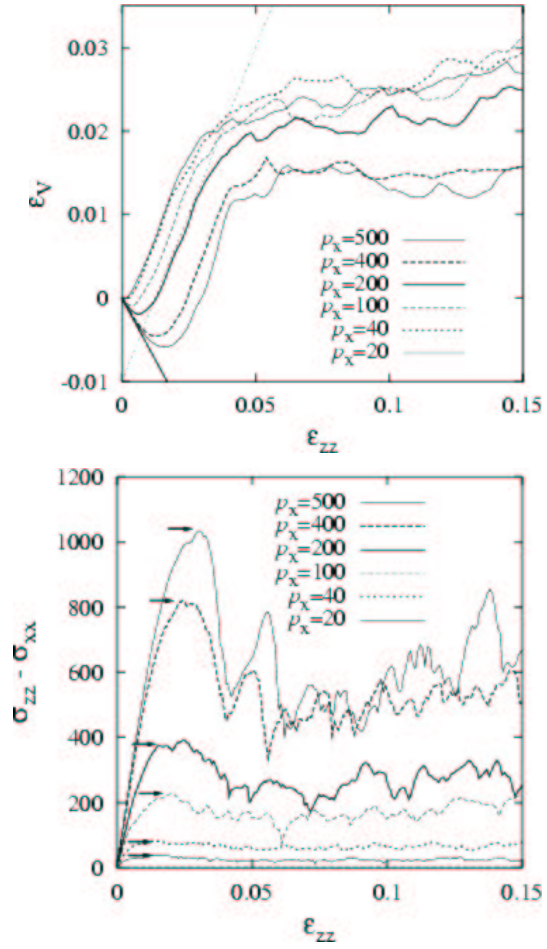

Figure 6: Volumetric strain (top) and stresses (bottom) during large deformations, both plotted against vertical strain, for different side pressure, as indicated in the inset. The peak yield stress is marked by arrows.

First, the vertical stress increases linearly; then the slope gradually decreases (softening), until the stress reaches its maximum (peak yield stress). After the peak, further softening/weakening behavior (with negative slope) is followed by a constant, strongly fluctuating stress for larger deformations.

It is possible to also examine the flow behavior of the system by plotting Mohr-circles for the maximum stress (right-most point on the circle) for different confining pressures (left-most point), see Fig. 7. The eigen-directions of the system are parallel to the walls, because there is no friction active between particles and walls, so that the left- and right-most points on the circles are indeed corresponding to the wall stresses; note that in an arbitrary geometry, it is not necessarily that simple. The tangent to the circles

(slope 0.588) can be seen as the flow function for peak stress. The corresponding friction angle is about 30.5^0 (26.6^0 expected from micro-friction). It is linear for the examined parameters, with its slope only slightly larger than expected from the microscopic friction at the contacts alone. Since we have not used cohesive forces, the macroscopic cohesion c is non-existent, i.e., the flow function hits the origin.

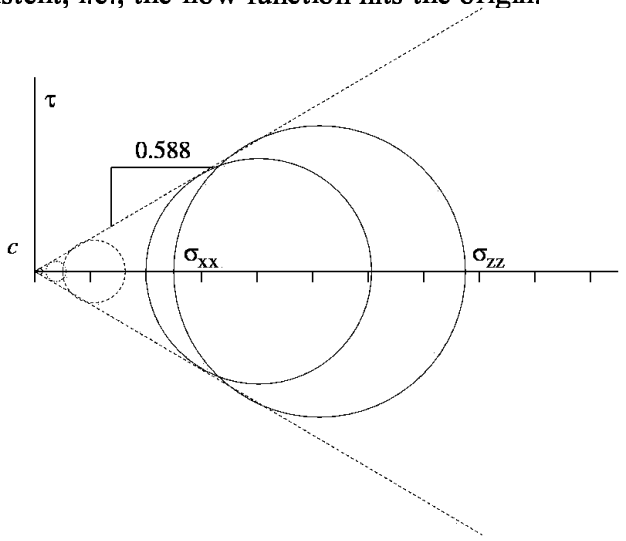

Figure 7: Mohr circle representation of the flow function at peak stress, see the arrows in Fig. 6 (bottom).

3.3 Macroscopic material parameters

From the simulation data presented in Figs. 4-7, it is possible to obtain the following material parameters, as based on an isotropy assumption:

(i) The initial slope (-0.59) of the volumetric strain allows to determine the Poisson ratio.

(ii) The slope of the volumetric strain in the dilatancy regime (+0.19 without friction, +0.80 with friction) is related to the dilatancy angle.

(iii) The initial slope of the stress is related to the bulk modulus (results not discussed further).

(iv) The peak (yield) stress is related to the flow function of the material. Interesting is a macroscopic friction angle that is always larger than the microscopic one.

3.4 Some material parameters for hypoplasticity

Some of the material parameters involved in a hypoplastic material theory [16-20] can also be extracted from the simulation data. An essential ingredient of the theory is the functional behavior of the pore number:

$$e^h = e_0^h \exp\left(-\left[p/h_s\right]^n\right) \qquad (5)$$

as a function of the pressure. The empirical model parameters for this function (based on experimental findings) involve the pore number at vanishing stress, e_0^h, the so-called granular hardness, h_s, and an empirical power n.

The function in Eq. (5) is astonishingly close to the fit-function (6) for the initial and the critical state pore-number envelope, see Fig. 8:

$$e(e_0, n) = e_0 - \left[p/h_s\right]^n \qquad (6)$$

where the parameters e_0 and n can be read off from the inset, and the granular hardness was set equal to the spring stiffness $h_s = k_2 = 10^5$ in the DEM contact model. Eqs. (5) and (6) can be related to each other via a series expansion in the small variable p/h_s.

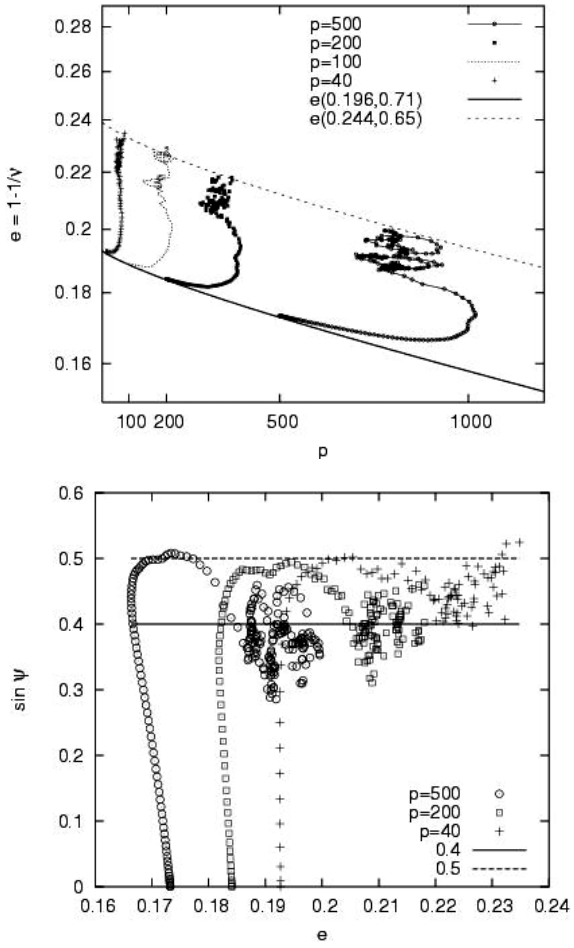

Figure 8: Pore number plotted against side stress (top), and deviatoric stress ratio plotted against pore number (bottom) – for different confining pressures.

The representation of the deviatoric stress ratio:

$$\sin\psi = \frac{\sigma_{zz} - \sigma_{xx}}{\sigma_{zz} + \sigma_{xx}} \qquad (7)$$

in Fig. 8 (bottom) is another way to extract the macroscopic friction angle. For peak stress, the simulations are almost in agreement with the microscopic friction coefficient μ=0.5, whereas for the critical state flow stress-value (besides strong scatter due to fluctuations), the macroscopic friction angle decreases with increasing pressure. For the largest pressure used here, the friction coefficient is smaller than μ_{cs}=0.4.

4 SUMMARY AND CONCLUSIONS

In summary, a set of DEM simulations was presented, and several macroscopic material parameters like, e.g., the friction angle, were extracted from the simulation data with cohesion (no friction) and with friction (no cohesion). Also the behavior of density (pore-number) and friction angle as function of the confining pressure were discussed and related to a hypoplastic material law [16-20].

The present results are a first step of a micro modeling approach for cohesive frictional powders. Further material parameters have to be identified, and also the dependence of cohesion has to be examined more closely, not only for frictionless [11-13], but also for frictional materials.

Also the role of particle rotations is an open issue, as related to micro-polar constitutive models. In both simulation and experiment, rotations are active in the shear band – like in micro-polar hypoplastic material models, where the rotational degree of freedom is activated in the shear band too. The corresponding parameter identification and the micro-macro-transition is another task for the future, like the implementation and simulation of experimentally determined force-laws [21] in three-dimensional systems.

ACKNOWLEDGEMENTS

This work was funded by the Deutsche Forschungs-gemeinschaft (DFG) in the framework of the research-group: "Verhalten Granularer Medien"; we acknowledge helpful and inspiring discussions with M.-K. Müller, K. Nübel, R. Pitchumani, and J. Tejchman.

REFERENCES

[1] H. J. Herrmann, J.-P. Hovi, and S.Luding, eds., *Physics of dry granular media*, NATO ASI Series E 350, Kluwer Academic Publishers, Dordrecht, 1998.

[2] P. A. Vermeer, S. Diebels, W. Ehlers, H. J. Herrmann, S. Luding, and E. Ramm, eds., *Continuous and Discontinuous Modelling of Cohesive Frictional Materials*, Lecture Notes in Physics 568, Springer, Berlin, 2001.

[3] Y. Kishino, ed., *Powders & Grains 2001*, Balkema, Rotterdam, 2001.

[4] C. Thornton and S. J. Antony, Quasi-static deformation of a soft particle system, Powder Technology 109(1-3), 179—191, 2000.

[5] G. A. D'Addetta, F. Kun, E. Ramm, *On the application of a discrete model to the fracture process of cohesive granular materials*, Granular Matter 4 (2), 77-90 2002.

[6] M. Oda and K. Iwashita, *Study on couple stress and shear band development in granular media based on numerical simulation analyses*, Int. J. of Enginering Science 38, 1713-1740, 2000.

[7] N. P. Kruyt and L. Rothenburg, *Statistics of the elastic behavior of granular materials*. Int. J. of Solids and Structures 38, 4879—4899, 2001.

[8] S. Luding, M. Lätzel, W. Volk, S. Diebels, and H. J. Herrmann, *From discrete element simulations to a continuum model*, Comp. Meth. Appl. Mech. Engng. 191, 21-28, 2001.

[9] J. Tomas, *Assessment of mechanical proper-ties of cohesive particulate solids – part 1: particle contact constitutive model*, Particulate Sci. Technol. 19, 95-110, 2001.

[10] J. Tomas, *Assessment of mechanical properties of cohesive particulate solids – part 2: powder flow criteria*, Particulate Sci. Technol. 19, 111-129, 2001.

[11] R. Tykhoniuk, and J. Tomas, *Simulation der Scherdynamik von kohäsiven Pulvern*, Chem. Ing. Techn. 75, (in press) 2003.

[12] S. Luding and H. J. Herrmann, *Micro-Macro Transition for Cohesive Granular Media* ,in: Zur Beschreibung komplexen Materialverhaltens, Institut für Mechanik, S. Diebels (Ed.), Stuttgart, 121--134, 2001.

[13] S. Luding, R. Tykhoniuk, and Jürgen Tomas, *Anisotropic material behavior in dense, cohesive powders*, Chem. Eng. Tech. 26(12), 1229-1232, 2003.

[14] M. Lätzel, S. Luding, H. J. Herrmann, D. W. Howell, and R. P. Behringer, *Comparing Simulation and Experiment of a 2D Granular Couette Shear Device,* Eur. Phys. J. E 11, 325-333, 2003.

[15] M. Oda, *Micro-fabric and couple stress in shear bands of granular materials*, in: Powders and Grains, C. Thornton, ed., Rotterdam, Balkema, 161-167, 1993.

[16] J. Tejchman and W. Wu, *Numerical study on patterning of shear bands in a Cosserat continuum*, Acta Mechanica 99: 61-74,1993.

[17] E. Bauer and W. Huang, *Numerical study of polar effects in shear zones*, in: Numerical Models in Geomechanics, G.N. Pande, S. Pietruszczak, H. F. Schweiger, eds., Balkema, 133-141, 1999.

[18] E. Bauer, *Calibration of a comprehensive hypoplastic model for granular materials,* Soils and Foundations 36, 13-26, 1996.

[19] J. Tejchman, *Patterns of shear zones in granular materials within a polar hypoplastic continuum*, Acta Mechanica 155, 71-95, 2002.

[20] K. Nübel, *Experimental and Numerical Investigation of shear localization in granular material*, PhD thesis, Karlsruhe, 2002.

[21] M. Kappl, H. J. Butt, *The colloidal probe technique and its application to adhesion force measurements*, Particle & Part. Sys. Charact. 19 (3), 129-143, 2002.